

Spontaneous Chiral Symmetry Breaking and Lane Formation in Ferromagnetic Ferrofluids

Mojca Vilfan,* Borut Lampret, Žiga Gregorin, Luka Cmok, Andrej Vilfan, Jürgen Klepp, Joachim Kohlbrecher, Patricija Hribar Boštjančič, Darja Lisjak, and Alenka Mertelj

Ferromagnetic ferrofluids are synthetic materials consisting of magnetic nanoplatelets dispersed in an isotropic fluid. Their main characteristics are the formation of stable magnetic domains and the presence of macroscopic magnetization even in the absence of a magnetic field. Here, the authors report on the experimental observation of spontaneous stripe formation in a ferromagnetic ferrofluid in the presence of an oscillating external magnetic field. The striped structure is identified as elongated magnetic domains, which exhibit reorientation upon reversal of the magnetic field. The stripes are oriented perpendicular to the magnetic field and are separated by alternating flow lanes. The velocity profile is measured using a space–time correlation technique that follows the motion of the thermally excited fluctuations in the sample. The highest velocities are found in the depleted regions between individual domains and reach values up to several $\mu\text{m s}^{-1}$. The fluid in adjacent lanes moves in the opposite directions despite the applied magnetic field being uniform. The formation of bidirectional flow lanes can be explained by alternating rotation of magnetic nanoparticles in neighboring stripes, which indicates spontaneous breaking of the chiral symmetry in the sample.

1. Introduction

Active matter describes nonequilibrium materials in which locally injected or stored energy is continually converted into motion. Its complexity increases immensely with the introduction of chirality.^[1] In recent years, chiral active matter has been studied over a wide range of sizes, from nanoscale molecular motors^[2–4] and externally driven colloidal microparticles^[5,6] to microscopic chiral grains and macroscopic robots.^[7–10] Depending on the scale, chirality can enter the system either via molecular asymmetry,^[2,11] chiral geometry,^[10,12–14] surface-induced symmetry breaking^[15–17] or by rotation of particles driven by an external magnetic field.^[5,18–21] The intriguing diversity of chiral active matter manifests itself in the rich variety of newly discovered phenomena, most notably long-range synchronization and flocking,^[22–25] active turbulence,^[26] emergence of spontaneous flow and edge currents,^[19,27,28] odd viscosity,

which causes flow perpendicular to applied stress,^[18,29,30] and the related odd elasticity.^[31,32] Possibly the most extensively studied approach in the quest for understanding these intricate phenomena is the use of an alternating magnetic field as the external source of energy. The application of an external magnetic field ensures not only reproducible experimental conditions but also control over inter-particle interactions, creating an important step toward understanding these complex systems.

Ferromagnetic ferrofluids are fluids that retain spontaneous magnetization in the absence of a magnetic field. Although their existence had been hypothesized for a long time,^[33–35] their realization only occurred less than a decade ago.^[36] Conventional ferrofluids, which are widely known for their magneto-viscous effects and intriguing surface instabilities when placed in an external magnetic field,^[37] are usually prepared as suspensions of spherical ferro/ferrimagnetic nanoparticles in isotropic solvents. In the absence of an external magnetic field, the orientation of particle magnetic moments is randomly distributed due to thermal energy; therefore, ferrofluid materials do not retain a remanent magnetization, and their response is, strictly speaking, superparamagnetic.^[38]

By replacing spherical nanoparticles with single-domain magnetic nanoplatelets in which the magnetic moment always points perpendicular to the platelet plane, a true liquid ferromagnet is


M. Vilfan, B. Lampret, Ž. Gregorin, L. Cmok, A. Vilfan, P. Hribar Boštjančič, D. Lisjak, A. Mertelj
J. Stefan Institute
Ljubljana 1000, Slovenia
E-mail: mojca.vilfan@ijs.si

M. Vilfan
Faculty of Mathematics and Physics
University of Ljubljana
Ljubljana 1000, Slovenia

A. Vilfan
Max Planck Institute for Dynamics and Self-Organization (MPIDS)
37077 Göttingen, Germany

J. Klepp
Faculty of Physics
University of Vienna
Vienna 1090, Austria

J. Kohlbrecher
Laboratory for Neutron Scattering and Imaging, PSI
Villigen 5303, Switzerland

 The ORCID identification number(s) for the author(s) of this article can be found under <https://doi.org/10.1002/smll.202304387>

© 2023 The Authors. Small published by Wiley-VCH GmbH. This is an open access article under the terms of the Creative Commons Attribution-NonCommercial License, which permits use, distribution and reproduction in any medium, provided the original work is properly cited and is not used for commercial purposes.

DOI: 10.1002/smll.202304387

obtained, which retains magnetization even when no magnetic field is applied. Initially, these magnetic nanoplatelets were introduced into a nematic host.^[39] Further investigations have shown that the combined effect of the particle shape, which induces strongly anisotropic steric interactions,^[40] and the interactions between particles' magnetic moments, which promote parallel orientation between neighboring particles, can also lead to a stable ferromagnetic ordering in an isotropic solvent at sufficiently high particle concentrations. In this ferromagnetic ferrofluid, the platelets and their magnetic dipole moments are locally on average oriented in the same direction, resulting in a stable suspension with spontaneous magnetization at room temperature. As such spontaneous orientational order without long-range positional order is characteristic for nematic liquid crystals, these materials are also known as ferromagnetic colloidal nematics.

Similarly to solid ferromagnets, ferromagnetic fluids have a strong tendency to form magnetic domains separated by domain walls.^[41] As the magnetic domains correspond to regions within which the magnetic dipole moments display polar order, in ferromagnetic nematics, this translates into regions with uniform platelet orientation. The orientation of magnetic moments, and thus the orientation of the magnetic platelets, can be switched by applying a static external magnetic field.

Here, we report on spontaneous chiral symmetry breaking in a ferromagnetic nematic ferrofluid in an oscillating external magnetic field. While switching of the initially formed domains is expected, under certain conditions, we observe a profoundly different behavior where stripes of particles assume rotation in opposite directions, resulting in the formation of flow lanes with alternating directionality between the stripes. Because the applied magnetic field is uniaxial, persistent rotation is a clear signature of spontaneous symmetry breaking. Such a ferromagnetic ferrofluid is thus interesting not only as a liquid magnet but also serves as a model system for pattern formation and symmetry breaking in active matter. The bidirectional flow lanes bear unique potential for a variety of tubeless microfluidic applications.

2. Results and Discussion

Ferromagnetic ferrofluids were prepared as suspensions of magnetic nanoplatelets in *tert*-butanol. The barium hexaferrite nanoplatelets had a mean diameter of $2r \approx 55$ nm and a thickness of $b \approx 4$ nm. Besides shape, their most important feature is their high magnetic anisotropy, with their magnetic moment constrained to the direction perpendicular to the particle plane.^[42–44] The particles can be characterized with the following parameters. The Langevin parameter that gives the ratio between the magnetic energy in an external field (magnetization M times particle volume V times the applied field B) and the thermal energy has a value of $\xi = MVB/(k_B T) = 1.1$ in a typical magnetic field of $B = 3$ mT. The strength of magnetic dipole–dipole interactions can be estimated by calculating the critical density for the transition to the ferromagnetic phase using the mean field (Curie–Weiss) theory as $\rho_c^* = 3k_B T/(\mu_0 M^2 V) = 4$ vol% (note that the mean-field theory underestimates the critical volume fraction,^[35] but steric effects also reduce it). Finally, the characteristic concentration above which steric effects dominate can be estimated as the ratio between the volume of a platelet and the excluded vol-

ume between two randomly oriented platelets,^[45] $\pi r^2 b/(4\pi r^3) = b/(4r) = 4$ vol%. These estimates suggest that both magnetic and steric interactions are in a range where they can lead to a phase transition to an ordered state. Indeed, anisotropic magnetic interparticle interactions lead to the formation of an orientationally ordered nematic phase at sufficiently high particle concentrations even in a zero external magnetic field.

Due to the optical birefringence of the nematic order, the orientationally ordered regions are easily identified under a polarizing microscope (POM). Taking into account that the POM transmittance $I \propto \sin^2(2\varphi)$, where φ is the in-plane angle between the locally averaged particle orientation (director) and the polarizer, the individual ordered regions of the sample generally appear bright when placed between crossed polarizers. Zero POM transmittance is obtained when the director is either parallel or perpendicular to the polarizer, or when the observed material is isotropic with no preferred in-plane orientation. This makes POM observations ideal for identification, characterization, and visualization of nematic order and, therefore, in our case, also of magnetic domains.

Observing samples with different concentrations of nanoplatelets in zero-magnetic-field conditions, we determined the threshold particle concentration for ferromagnetic phase formation to be approximately 5–6 vol%. Above this value, at least partial local ordering of the platelets was observed in the sample. The obtained threshold concentration is significantly lower than 28 vol%, which was originally reported by Shuai et al.^[36] The substantial reduction in the critical volume fraction was achieved by excluding smaller platelets and optimizing the parameters of the suspensions, as described previously.^[46] Additional evidence that the observed birefringence was indeed a consequence of spontaneous platelet ordering was the appearance of the so-called schlieren structure, which is typical for an unaligned nematic, indicating only locally uniform order (Figure 1a).

When the material was placed in a weak magnetic field of 1.3 mT, large domains appeared (Figure 1b). The domains with a characteristic size of several hundreds of micrometers were separated by clearly visible domain walls and could be switched by changing the direction of the applied external magnetic field. In contrast to solid ferromagnets, in which the magnetic easy axis is pinned to the crystal structure, the easy axis in fluid ferromagnets can continuously change direction, together with the local average orientation of the platelets described by the nematic director. The reorientation of the magnetization corresponds to the reorientation of the platelets, which is observed as a change in the intensity of the transmitted POM light. Upon switching direction of the applied magnetic field, the initially dark regions become bright and vice versa (Figure 1c). Similar behavior has been observed in thin capillaries, where formation and slow switching of magnetic domains has been studied in detail.^[41]

2.1. Spontaneous Stripe Formation

When the ferromagnetic colloidal nematic was placed in an oscillating magnetic field, the observed behavior was completely different from that in a static magnetic field. Applying an external magnetic field with an amplitude B_0 of up to 10 mT with

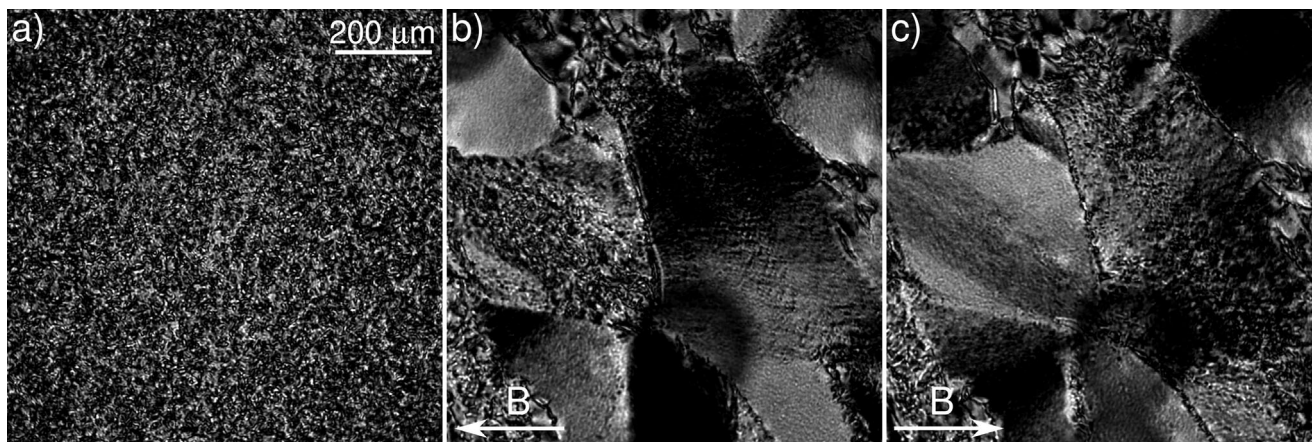


Figure 1. Ferromagnetic nematic phase under a polarizing microscope. a) In zero external magnetic field, the observed schlieren structure indicates the existence of nematic phase. b) When placed in a weak magnetic field ($B = 1.3$ mT), large domains appear. c) Switching of the domains by changing the direction of the field. The change in magnetization orientation is seen as a change in the POM transmittance. The scale is the same for all panels.

frequencies up to 25 Hz in the direction parallel to the sample plane, for a rather narrow interval of field parameters, very unusual striped structures were observed under polarizing microscope. **Figure 2** shows POM images that were recorded at increasing field amplitudes for two different oscillation frequencies: top row (a–g) at a frequency of 1 Hz and bottom row (h–n) at 5 Hz, at a particle concentration of 12 vol%. The sampling was locked to the oscillating field, so that all images were taken when the magnetic field reached the peak value of B_0 within the oscillation cycle. A waiting time of 30–60 s between each measurement ensured that the images were recorded in steady state.

At low magnetic field amplitudes, nematic defects in the structure prevailed and the acquired images are typical for the unaligned nematic phase (a,h). Upon increasing the amplitude of

the oscillating magnetic field, the ordered areas grew (b,i) and visible lines emerged in the direction perpendicular to the magnetic field (c,j). The lines then grew in length and became more pronounced (d,k–m). An additional increase in the field amplitude reduced the line visibility (e,f,n), until they disappeared completely and the sample became homogeneous (g). At 5 Hz, the field at which the lines disappeared exceeded the observation range.

The experiments reveal that the stripes always form in the direction perpendicular to the oscillating magnetic field in a relatively narrow interval of magnetic field strengths and frequencies (Figure 2 r). The magnetic field at which the stripes appear is almost independent of the field frequency (a variation of 20–30% was observed at larger concentrations), whereas the field at

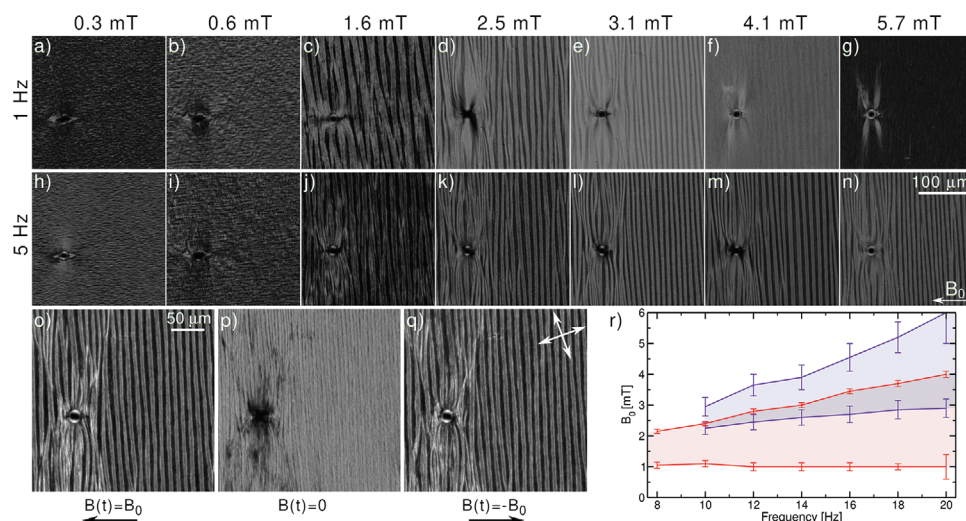


Figure 2. Ferromagnetic fluid under a polarizing microscope in an oscillating magnetic field. a–g) Images taken at increasing oscillation amplitude at 1 Hz and h–n) at 5 Hz. The magnetic field points in the horizontal direction, and all images were taken when the field strength reached its maximum value B_0 . o–q) Images taken during one half of the oscillation period with the magnetic field pointing to the left, at zero-crossing, and at field pointing to the right, respectively, at 10 Hz and $B_0 = 3.1$ mT. Particle concentration in (a–q) was 12 vol%. The crossed arrows indicate orientations of the polarizers. The visible line distortions in POM images occur around a 20 μm spherical spacer. r) Phase diagram of oscillation frequencies and magnetic field amplitudes at which striped structure appears for 5 vol% (red) and 8 vol% (blue).

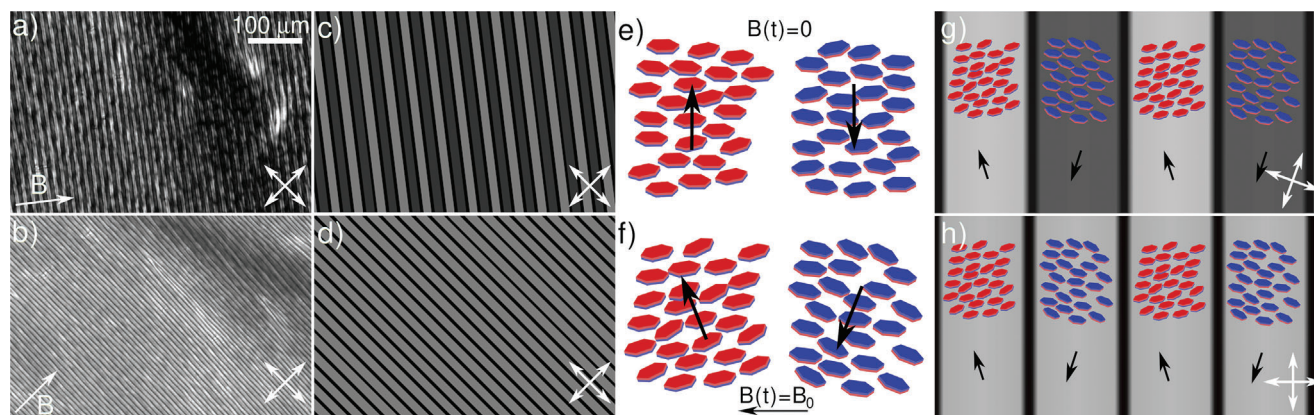


Figure 3. Proposed platelet configuration based on POM rotation images. a) The oscillating magnetic field ($B_0 = 3.8$ mT and 10 Hz at 12 vol%) is rotated relative to the polarizers and b) the field is parallel to one of the polarizers. c,d) Simulated POM transmittance, which matches the observed patterns. e) Proposed platelet configuration at zero value of the oscillating field, and f) proposed platelet configuration in the magnetic field pointing to the left. g,h) Platelet orientations and difference in transmittance explained for different orientations of crossed polarizers.

which the stripes disappear steadily increases, for example, from 3 mT at 10 Hz to over 5 mT at 20 Hz at a concentration of 8 vol%. In general, lower particle concentrations require lower magnetic fields for the stripes to form, whereas at higher concentrations (above 10%), the stripes remained visible beyond the maximum applied magnetic field of 10 mT. The stripe periodicity is found to be around 12 ± 3 μm (mean \pm s.d.) and within experimental error independent of the magnetic field amplitude. It does, however, increase with the particle concentration, from around 8 μm at the threshold, to a maximum of 14 μm .

An important stripe characteristic is their behavior upon reversal of the magnetic field, as shown in Figure 2o–q. When the magnetic field changes direction, the striped pattern remains visible, but the previously bright stripes in (o) turned dark in (q) and vice versa. However, when the field crossed the zero-field value (p), the sample appeared much more homogeneous, with only very thin black stripes present.

To analyze the striped pattern and obtain information on the particle orientation within the stripes, additional POM observations were made in which the polarizers were rotated against the direction of the magnetic field (Figure 3a,b and Supporting Information). Based on the POM transmittance going to zero when the director is parallel to one of the polarizers (Figure 3a), we estimated by observation of the acquired images that for given field parameters, the director oscillated toward and against the direction of the stripes for around 20° , alternatingly in neighboring stripes. When the polarizers were symmetrically oriented with respect to the stripe direction (Figure 3b), the periodicity of the sample changed, as previously observed stripes now exhibited equal transmittance, with only thin black lines remaining. These thin black lines remained unaffected by the polarizer rotation, indicating that the black stripes are optically isotropic.

Based on these observations, we propose a director configuration for the striped pattern as follows (Figure 3e,f). Individual bright stripes correspond to regions of the same average particle orientation, and thus represent individual magnetic domains. The elongated domains are separated by thin lines, which remain black regardless of the sample orientation and can therefore only be regions of isotropic material. Since they separate in-

dividual oriented magnetic domains, we call these regions domain walls.^[41] In contrast to observations in highly concentrated samples,^[36] these domain walls are much thinner with no internal twist structure visible. For the domain walls to be isotropic, either the nanoparticles within them have to be randomly oriented or these walls represent regions with very low particle concentrations—possibly even without them. Our experimental findings support the latter explanation, as already at very low concentrations (below 1 vol%) the particles tend to locally order and show birefringence in fields as low as the Earth's magnetic field. We find it unlikely for the applied magnetic field to be so low between the stripes throughout the whole cycle, especially for magnetic fields as strong as 10 mT. We thus favor the explanation that the domain walls are depleted regions with low concentrations of magnetic nanoparticles.

A comparison of the acquired images with a simple POM simulation is shown in Figure 3c,d. In the simulation, the local director orientation, orientations of the polarizers, and the optical anisotropy of the material were taken into account. The director orientation was considered to be planar, with thin lines of homeotropic alignment in between mimicking depleted isotropic regions. The director in neighboring bright stripes was alternately oriented at an angle of 20° and -20° relative to the stripes. The calculated transmitted light pattern shows an excellent correspondence with the actual POM images, reproducing both the difference in stripe transmittance and the change in periodicity upon rotation. Accordingly, Figure 3g,h depicts the particle orientation in individual stripes, consistent with equal transmission when the polarizers are symmetric and alternately dark and bright otherwise.

We should add that stripe formation is not instantaneous. The transient dynamics of stripe formation upon switching on the magnetic field is shown in Figure 4a–f and a POM movie in Supporting Information. The mean length of the stripes was measured as a function of time for various field amplitudes (Figure 4g) and different field oscillation frequencies (Figure 4h). The characteristic stripe formation time, which was estimated as the time, after which the average stripe length no longer significantly increases, was found to range from ≈ 10 s at

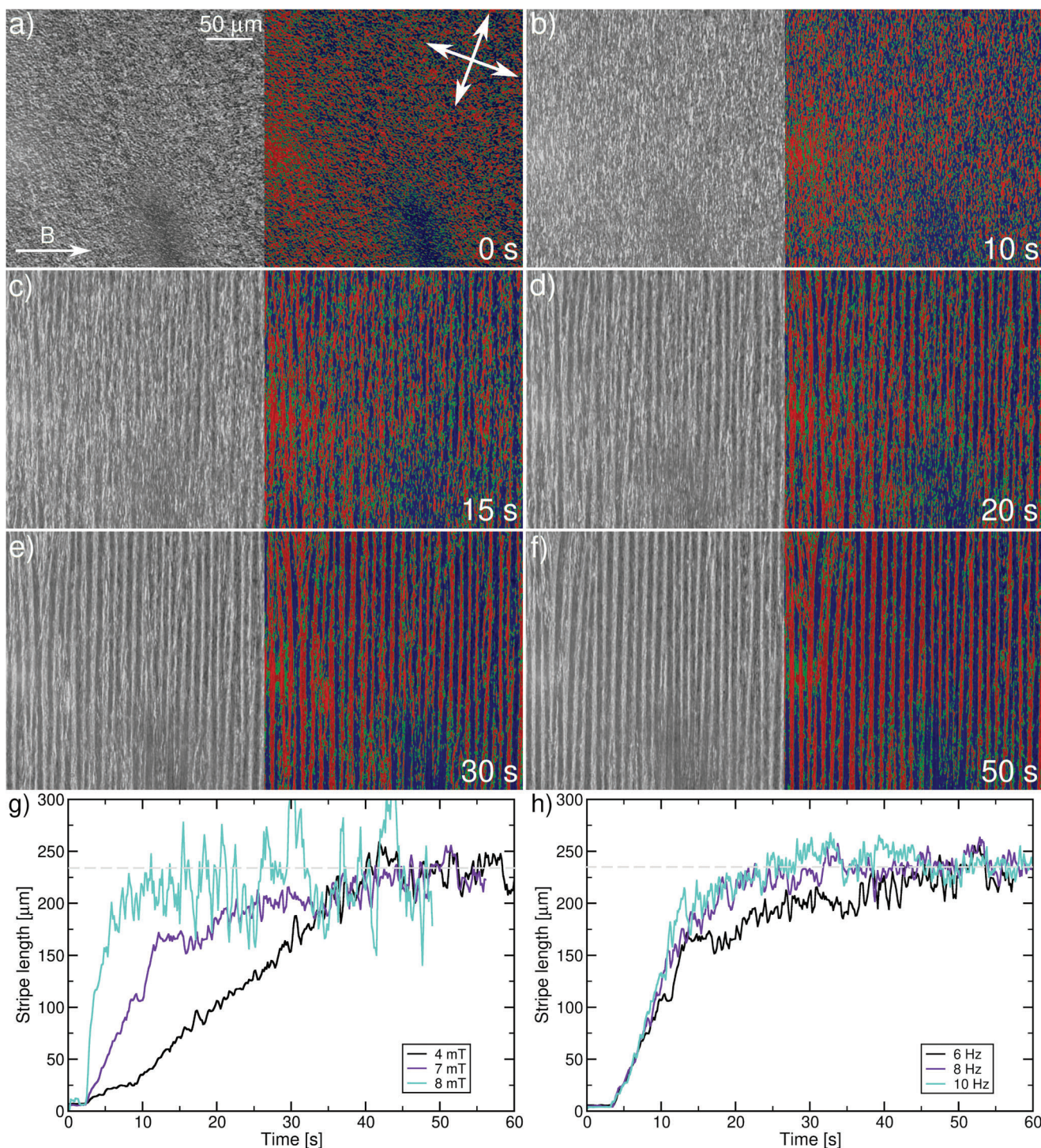


Figure 4. Formation of stripes upon switching on the oscillating magnetic field. a–f) Time development of the formation, with grayscale images being direct POM images and RGB images depicting the heatmap of deviation from the average transmittance (blue is minimal, and red is maximal transmittance). g) Average stripe length as a function of time for three values of the magnetic field amplitude at an oscillation frequency of 6 Hz. h) Average stripe length as a function of time for three oscillation frequencies at $B_0 = 7$ mT. Particle concentration was 10 vol%.

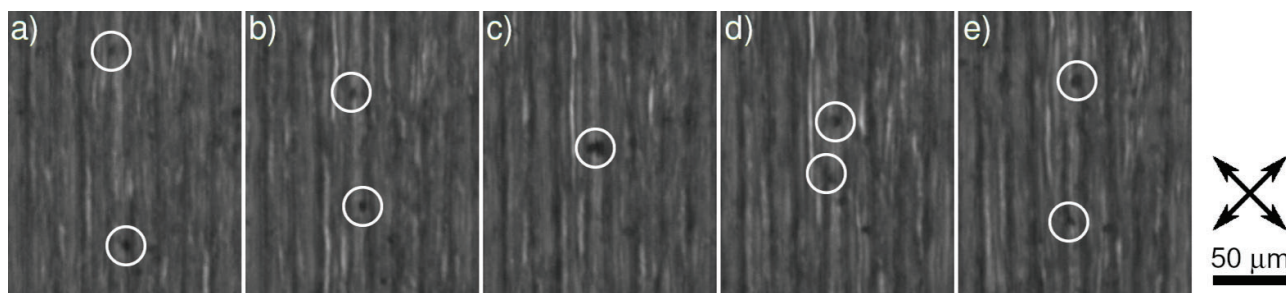


Figure 5. A sequence of images showing the motion of aggregates along the stripes in the direction perpendicular to the oscillating horizontal magnetic field. a) $t = 0$, b) $t = 14$ s, c) $t = 30$ s, d) $t = 42$ s, and e) $t = 55$ s at $B_0 = 3.7$ mT, 10 Hz, and 10 vol%. Arrows indicate the direction of POM polarizers. The particles in the neighboring stripes move in the opposite direction with an estimated velocity of $2 \mu\text{m s}^{-1}$.

$B_0 = 8$ mT to ≈ 40 s at $B_0 = 4$ mT, thus exhibiting a strong field dependency. The formation time, however, was found to be almost independent of the field oscillation frequency.

2.2. Bidirectional Flow Along the Stripes

A close examination of the observed stripes reveals that for certain field amplitudes (typically around 0.5 mT above the threshold for stripe formation), the striped structure is not stationary. Initially spotted as the motion of individual randomly formed aggregates, we were able to observe the motion in the sample plane in the direction perpendicular to the magnetic field (Figure 5 and Supporting Information). Surprisingly, individual aggregates in neighboring stripes moved in opposite direction, despite the external oscillating magnetic field being uniaxial. The aggregates appeared to move within or in the vicinity of black lines, previously identified as isotropic depleted areas, with an estimated velocity of around $2.5 \mu\text{m s}^{-1}$.

The observed flow suggests that there are two regimes of the striped sample structure. One regime is the wobbling described in the previous section, in which the particles oscillate by a relatively small angle (for example $\pm 20^\circ$ for the parameters shown in Figure 3). Another regime appears in a stronger magnetic field, in which the oscillation amplitudes increase and in which net flow is observed.

Since the aggregates that we observed in motion were magnetic and fairly large, their propulsion may not correspond to the actual flow in the fluid. We therefore employed a space–time correlation microscopy method to investigate the appearance of the flow lines along the stripes. In contrast to standard velocimetry methods, in which tracer particles are introduced into the system and their movements monitored, this approach is based on following the thermally excited long-wave fluctuations in the sample structure rather than individual particles. Due to the finite fluctuation relaxation time, the method works best for relatively short observation times, but detects also long-lived inhomogeneities in the sample and, more importantly, avoids using the tracer particles completely, which would disturb the particle ordering and influence the sample dynamics.

To understand the dynamics in the sample, a detailed velocity profile was acquired by tracking the fluctuations in the direction parallel to the stripes. By calculating the correlation functions of time-dependent signals and following their max-

ima, we obtained the relation between displacement Δy and time delay Δt of the observed pattern, as shown in Figure 6a for one given trace. The linear fit of this relation yields the corresponding average velocity. The presented histogram shows that although the majority of the fluctuations were short-lived, contributing to the measurements within the first second, patterns longer than 10 s were also observed. However, these events were rare as the probability of structural changes increased to the point that individual correlation peaks could no longer be reliably followed, and the peak tracing needed to be restarted.

Two examples of the measured average flow velocity profiles are presented in Figure 6b,c for two different values of the magnetic field parameters. They clearly demonstrate that the largest average flow velocity is exhibited in the dark domain walls. In these depleted regions, the concentration of the magnetic nanoparticles is the lowest, and correspondingly, the viscosity is minimal. Flow velocities in these regions reach values of up to $8 \mu\text{m s}^{-1}$, with symmetrically similar values in the opposite direction in neighboring dark stripes. We find that the flow velocity depends strongly on the strength of the magnetic field (Figure 6 d): For low fields, below approximately 2.5 mT, there is no net flow in the stripes, whereas for fields above 4 mT the magnetic field orients the platelets and the stripes are no longer observed. The magnetic field interval, in which the flow in the stripes is observed, depends also on the frequency of the magnetic field oscillations, with a slight increase observed with increasing frequency. The measured interval at 10 Hz is thus around 2.5–3.5 mT and around 3–4 mT at 18 Hz. The flow, which appears in the stripes, significantly contributes to the alignment of the domains and the stabilization of the striped structure. However, we believe that even in the wobbling regime, the small induced oscillating flow can have similar effect on the striped structure, and although no net flow is observed in the wobbling regime, there is enough local oscillating flow to stabilize the striped domain structure.

The formation of flow lanes in a mixture of clockwise and counterclockwise rotating surface-bound spinners has recently been predicted on theoretical grounds.^[47] In the model studied, individual spinners have a prescribed sense of rotation and then segregate into striped domains. Here, our system differs crucially, as the particle rotation is also the result of spontaneous symmetry breaking, which we discuss in the following section.

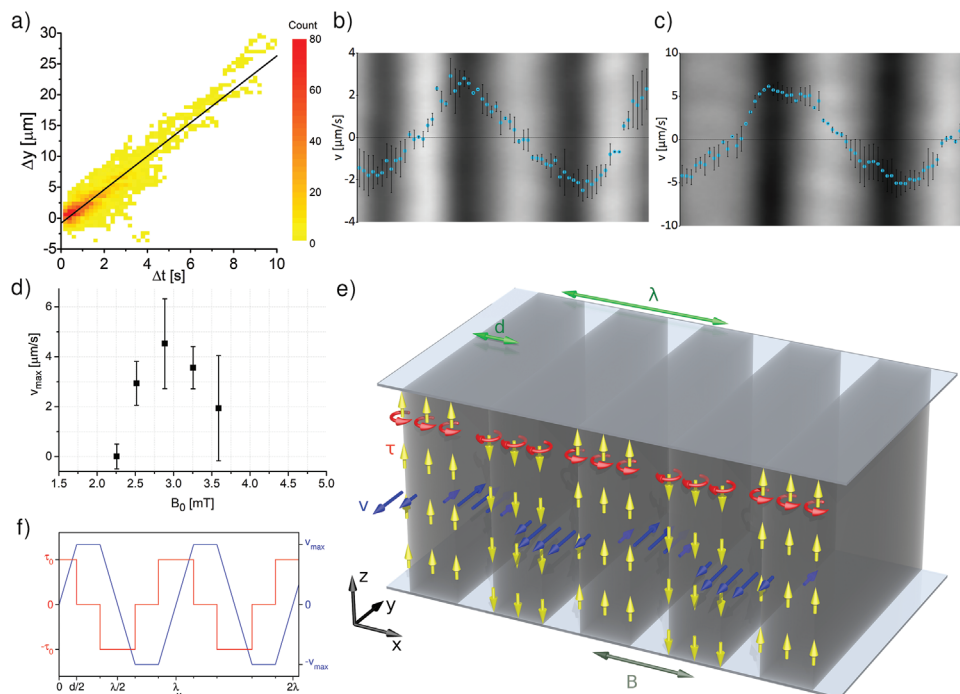


Figure 6. Flow in the striped structure. a) The flow velocity along the striped structure was determined by fitting the distribution of the cross-correlation peak positions Δy versus time delay Δt . The slope of the fitted line corresponds to the flow velocity along one $0.23 \mu\text{m}$ wide pixel line parallel to the observed stripes. b,c) Obtained flow velocity profiles at 3.0 and 3.3 mT, respectively, at 14 Hz and 8 vol%. Image width is $15 \mu\text{m}$. d) Maximum measured velocity as a function of magnetic field amplitude at 10 Hz field oscillation frequency. e) Proposed hydrodynamic model. The magnetic particles are concentrated in stripes of thickness d (dark) where they rotate (red arrows) and exert a torque density τ in alternating directions (yellow arrows). The torque distribution leads to flow lanes with a velocity profile indicated by blue arrows. The velocities are maximal in the depleted areas between stripes. f) The torque density profile (red) along the direction of the magnetic field (x) and the corresponding lateral flow velocity (blue).

2.3. Spontaneous Chiral Symmetry Breaking

To understand the origin of the observed flow, a microscopic view of this complex and nonhomogeneous system must be considered. We have previously established that bright stripes represent ferromagnetic domains with adjacent antiparallel ordering and dark stripes the depleted domain walls. Based on this model, the mechanism for the flow and its dependence on the magnetic field amplitude can be explained as follows. When the amplitude of the applied oscillating magnetic field is rather small (but large enough for the stripes to appear), the maximum angles of platelet wobbling are rather small and the nanoplatelets oscillate around the stationary antiparallel orientation. A too large magnetic field, on the other hand, reorients and redistributes the particles so that striped patterns no longer appear.

In the narrow intermediate regime, both the stripes and the flow are observed, which can only be explained by spontaneous chiral symmetry breaking occurring in the samples. Instead of just oscillating back and forth, the rotation angles of the nanoplatelets in this interval of magnetic field amplitudes are sufficiently large for the platelets to start rotating. Once the rotary motion starts locally, the collective rotations induce flow in the depleted regions surrounding the domain. The created flow induces rotation in the adjacent domain in the opposite direction, resulting in formation of stable flow along the domain walls (Figure 6e).

Additional information on platelet ordering and orientation was acquired by small-angle neutron scattering (SANS) experiments,^[48,49] carried out at the Swiss spallation neutron source at the Paul Scherrer Institute in Villigen, Switzerland. We previously used the method to observe the evolution of short-range positional and orientational magnetic order in a static external magnetic field.^[44] Expanding the technique to stroboscopic measurements and synchronizing the detection with the oscillation frequency of the magnetic field, we were able to detect the variation of neutron scattering patterns during the complete oscillation cycle. However, since the neutron beam size was of the order of several millimeters and thus much larger than the sample periodicity, local dynamics could not be observed, but rather an average over a large number of individual domains. As shown in Figure 7a, the sample was vertical in the xy plane, with the neutrons propagating along the z direction and an oscillating magnetic field applied along the x axis.

Figure 7b–d shows neutron scattering patterns for three different amplitudes of the oscillating magnetic field, taken at the moment when the magnetic field reached its maximum value. In the small magnetic field of 0.05 mT (b), the scattering pattern shows weak and relatively broad peaks, which indicate a rather weak orientational correlation between the particles. The broad peaks, which are centered around $\phi = 0^\circ$ and 180° , indicate that the particles oscillated around their average orientation, which was perpendicular to the external magnetic field. In the intermediate field of 1.6 mT (c), the peaks shifted toward the direction

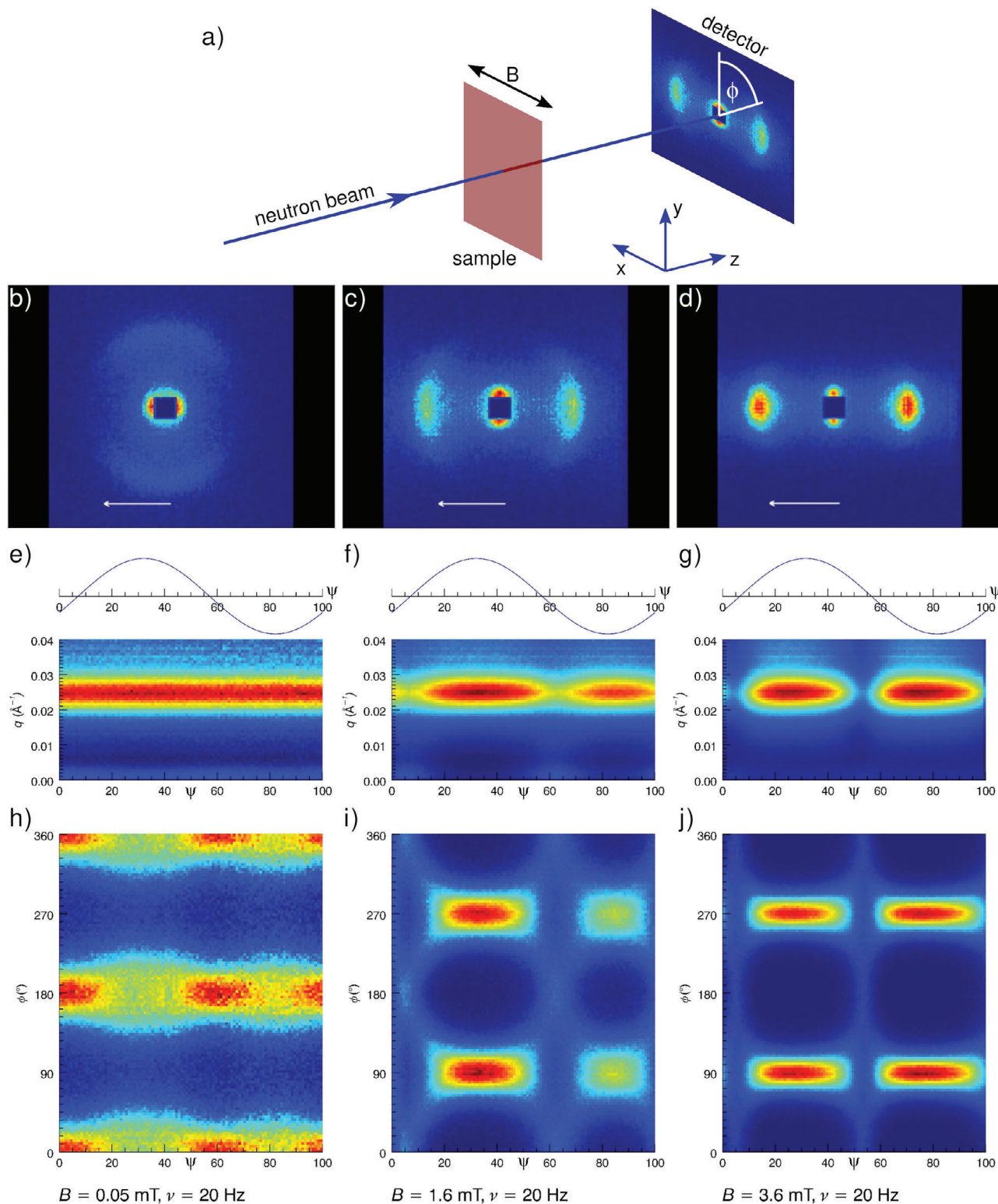


Figure 7. Small angle neutron scattering on ferromagnetic ferrofluids in an oscillating magnetic field. a) Experimental setup and orientation. b-d) Neutron scattering patterns obtained at $B_0 = 0.05$, 1.6 , and 3.6 mT, respectively, taken at $B(t) = B_0$ at 20 Hz with the magnetic field direction indicated by the arrows. Angular distribution of scattered neutrons corresponds to the angular distribution of the nanoplatelet magnetic moments. e-g) Scattering intensity averaged over the azimuthal angle during one oscillation cycle for the same magnetic field amplitudes. The cycle phase ψ is presented in units of $2\pi/100$. h-j) Matching azimuthal dependence at a wave vector that corresponds to the maximum scattering intensity. Zero azimuthal angle is perpendicular to the applied magnetic field.

of the external field, but remained rather broad. Since multiple domains were observed simultaneously, and the particle orientation in neighboring stripes oscillated in the counter-direction, the observed peaks are symmetric with respect to the direction of the magnetic field. In the strong magnetic field of 3.6 mT (d), the narrow peaks signify strong orientational correlations.

By averaging the intensity of the measured signal over the azimuthal angle ϕ in the xy plane and normalizing it by the scattering intensity at low concentrations to minimize the contribution of the particle form factor, the strengths of the interparticle correlations were obtained, as shown in Figure 7e–g. The abscissa shows one complete field oscillation cycle ψ , divided into 100 channels, and the ordinate the scattering wave vector. The observed peaks correspond to 23 nm at a concentration of 7 vol%, independent of the magnetic field amplitude. Observing the behavior within an oscillation period, we see that in the low field, the correlations remain constant during the whole cycle (e). In the intermediate field (f), the correlations are reduced when the field changes sign, but still non-zero, whereas in the strong field (g), the observed correlations disappear when $B(t) = 0$. The loss of correlation indicates that during the reorientation of the field, particles are in disarray before being oriented by the field in the opposite direction. The observed slight asymmetry is likely to be a consequence of a small bias field.

Limiting the observations to a small interval around the wave vector q , at which the scattering is the strongest, we analyzed the angular distribution of the acquired signal (Figure 7h–j). Corresponding to the direction of the particle magnetic moments, at low fields, a rather broad distribution is observed around the direction perpendicular to the magnetic field. The angular distribution is the largest when the field reaches its maximum value $B(t) = \pm B_0$, matching the particle configuration as shown in Figure 3f, and is visibly reduced at $B(t) = 0$, corresponding to the particle orientation shown in Figure 3e.

By increasing the field, the most prominent peaks shift from 0° and 180° to 90° and 270° (Figure 7i), with the peaks parallel to the magnetic field when the field reaches its maximum value. However, at $B(t) = 0$, a reorientation is visible, appearing like a brighter cross between the observed peaks. The cross-over between the peaks of maximum intensity clearly shows that the angles of rotation reach 90° and are thus large enough for the full rotation of particles to occur, rather than just wide-angle oscillation. The SANS observations therefore confirm the proposed model of rotating particles in neighboring domains in which the alternating direction of particle rotation occurs spontaneously in an oscillating uniform external magnetic field. Although the observed flow lines can be compared to the fluid transport along the spontaneously formed lines in suspensions of magnetic microplatelets observed by Solis and Martin,^[50,51] we should point out that their macroscopic system is inherently and conceptually different from ours. Not only is the scale over two orders of magnitude larger, making the system inertial and allowing the magnetic moments to rotate within the microparticles, the magnetic fields, in which the so-called isothermal magnetic advection occurred, were also bi- or triaxial. Due to the complexity of the systems, the authors did not provide a detailed explanation of the phenomenon but suggested complex hydrodynamic effects and coupling between the particles as the underlying mechanism.

Our experiments confirm that the rotation of the nanoplatelets indeed explains the creation of flow in the spontaneously formed stripes. To support and compare the model with a numerical calculation, we calculated the mean rotation frequency of the platelets from the velocity of the observed flows. In the following, we show a simple calculation that assumes that the sample thickness is larger than the distance between the stripes. An exact solution for a finite thickness is shown in the Supporting Information and only leads to a small correction (Figure S1, Supporting Information). We assume that the rotating particles are exerting a torque density $\tau(x, y, z)$, which has the value $\tau = \tau_0$ in even stripes ($-d/2 \leq x - n\lambda \leq d/2$), $\tau = -\tau_0$ in odd stripes ($-d/2 \leq x - \lambda/2 - n\lambda \leq d/2$) and $\tau = 0$ in the regions between the stripes (Figure 6f, red line). Because the cell width is several orders of magnitude larger than its height and the distance between the stripes, the flow takes the form $\mathbf{v} = v(x)\hat{e}_y$. Likewise, because of translational symmetry, the pressure p has to be constant along the stripes. The Stokes equation

$$\eta \Delta \mathbf{v} = \nabla p - \mathbf{f} \quad (1)$$

then takes the shape

$$\eta \partial_x^2 v_y = -f_y. \quad (2)$$

Here, the effective force density is determined by the gradient of the torque density, $f_y = -\partial_x \tau_z$.

These equations are solved by

$$v_y(x) = \begin{cases} (\tau_0/\eta)x & x \leq d/2 \\ \tau_0 d/(2\eta) & d/2 \leq x \leq \lambda/2 - d/2 \\ (\tau_0/\eta)(\lambda/2 - x) & \lambda/2 - d/2 \leq x \leq \lambda/2 + d/2 \\ -\tau_0 d/(2\eta) & \lambda/2 + d/2 \leq x \leq \lambda - d/2 \end{cases} \quad (3)$$

in the first period (Figure 6f). The model therefore predicts a velocity that is uniform between the stripes, with an alternating direction. Inside the stripes, the velocity changes linearly (Figure 6f, blue line). The torque density inside the stripes $\tau_0 = \rho \gamma_r 2\pi v_{\text{eff}}$ is determined as the number density of the particles $\rho = (\lambda/(2d))\rho_v/(\pi r^2 b)$, multiplied with the rotational drag coefficient $\gamma_r = (32/3)\eta r^3$ and the effective angular frequency $2\pi v_{\text{eff}}$. Together, the velocity between stripes is related to the mean rotation frequency as:

$$v_{\text{max}} = \frac{16\lambda\rho_v r}{3b} v_{\text{eff}}. \quad (4)$$

From the maximum velocity of $5 \mu\text{m s}^{-1}$, we estimate $v_{\text{eff}} = 0.14 \text{ Hz}$. The ratio between the rotation frequency and the field switching frequency can be used to estimate the bias in the platelet rotation upon the switching of field direction. A ratio of approximately 1:70 suggests that the rotation is largely random, as expected from thermal fluctuations, but a small bias of the order of a few percent breaks the symmetry and leads to the emergence of the self-sustained alternating flow lanes. Although the exact value is likely affected by the approximation in which we treated the magnetic suspension as a Newtonian fluid, the large ratio suggests robustness of the qualitative explanation.

A more accurate model of this complex system would additionally have to consider both the magnetic and electrostatic

interparticle interactions in the oscillating external magnetic field, combined with a large particle size polydispersity. This, however, is beyond the scope of the paper.

3. Conclusions

We have observed and studied the effect of spontaneous chiral symmetry breaking in recently discovered ferromagnetic ferrofluids when exposed to an oscillating external magnetic field. Manifested as a formation of visible striped patterns under the polarizing microscope, we established that the stripes, which formed in the direction perpendicular to the magnetic field, represented elongated magnetic domains of nematically ordered magnetic nanoplatelets. In the regions between the domains, which could be interpreted as domain walls, under certain conditions flow lanes were observed with the direction of flow alternating between the neighboring domain walls and reaching velocities of $5 \mu\text{m s}^{-1}$. Confirmed by SANS observations and compared to a simple hydrodynamic model, our study shows that the flow lanes appear due to spontaneous ordering and collective rotation of the magnetic nanoparticles within magnetic domains. The described ferromagnetic ferrofluids are thus not only interesting for their technological application potential as fluid magnets or in tubeless microfluidics, but also in fundamental research as they display an intriguing and rich complex behavior, previously unknown in active matter.

4. Experimental Section

Sample Preparation: Ferromagnetic colloidal ferrofluids were prepared as suspensions of magnetic nanoplatelets in *tert*-butanol at volume concentrations between 4% and 15%. As the concentrations were derived from magnetometric measurements, we estimate the relative error of the volume concentrations to be around $\pm 20\%$. The scandium-substituted barium hexaferrite magnetic nanoplatelets were synthesized hydrothermally at 245°C , as described previously^[42–44] and suspended in *tert*-butanol with DBSA as surfactant for stabilization (approx. 20 wt%). For SANS measurements, 1-butanol was used due to lower environmental temperature. Typical thickness of the platelets was about 4 nm and the diameter distribution approximately log-normal with a mean value of 55 nm and a standard deviation of 20 nm.^[43] The magnetization of the dried nanoplatelets was measured using a vibrating sample magnetometer (Lakeshore 7400 Series VMS) and found to be $(1.65 \pm 0.05) \times 10^5 \text{ Am}^{-1}$.

Commercially available sample cells (Instec, Inc.; rubbed polyimide) with a thickness of $20 \mu\text{m}$ were filled with suspensions of different concentrations. At low concentrations, capillary flow was strong enough, whereas the high viscosity of the more concentrated samples, combined with the comparatively rapid evaporation of the alcohol, required the samples to be filled under increased pressure through a capillary and isolated from the air. For SANS measurement, special fused quartz cells (EN08) were prepared at a thickness of $50 \mu\text{m}$ and $120 \mu\text{m}$.

Methods: The samples were observed optically under a polarizing microscope (Nikon Optiphot II) and images recorded with a CMOS digital camera (IDS Imaging UI-3370CP). To compensate the Earth's magnetic field, three orthogonal pairs of coils with pairwise individual current steering control were manufactured and an additional pair of coils within these zero-field coils was used to generate and control the external magnetic field acting on the sample. The applied field was always in the horizontal plane (parallel to the plane of the sample) with an amplitude of up to 30 mT above the zero-field value. The applied external field oscillated at a frequency in the range of 5–30 Hz and at an amplitude typically in the

range of 2–10 mT. Zero magnetic field conditions were probed by diluted samples, which remained in the isotropic phase and thus dark under POM.

Velocity within the stripes was measured by space-time correlation microscopy where images, taken at different times (but at the same phase of the field oscillations at $+B_0$), are compared to each other and correlations between the acquired POM images calculated. The flow velocity was then calculated from the obtained displacement of the maximum correlation peak and the time delay between the two images. Since a variation of velocity is expected in the direction perpendicular to the stripes, the flow was observed individually along pixel lines ($0.233 \mu\text{m}$ wide), which were chosen to be as parallel to the stripes as possible.

The correlation function for intensity signals $I_0(y, 0)$ and $I_t(y + \Delta y, \Delta t)$ can be written as:

$$(I_0 * I_t)(\Delta y, \Delta t) = \int_{y=-\infty}^{\infty} I_0(y, 0) I_t(y + \Delta y, \Delta t) dy \quad (5)$$

where y denotes the position in the direction of the flow and Δt the chosen delay in time, which is the time difference between two individual frames. By shifting the measured signal in y by Δy , the correlation function reaches a maximum value at a specific Δy , denoting the displacement of the pattern in the y direction in the given time delay of Δt . The velocity was then determined as the linear fit of the obtained $\Delta y(\Delta t)$ distribution for all the observed correlation peaks. The periodicity of the observed pattern allowed to follow several peaks simultaneously, yielding more reliable and reproducible values for the flow velocity. However, due to the soft and complex nature of the sample, demonstrating both thermal fluctuations and other slow variations in the sample structure, combined with pattern periodicity, the correlation approach could potentially give incorrect velocity values. To overcome the described problems, the correlation function was calculated between the initial image and all the images acquired at later times. Sudden jumps in the correlation function were avoided by manually excluding the shifts with velocities that are larger than five times the estimated maximum velocity.

Statistical Analysis: The data presented in Figure 2r (the phase diagram for striped structures) are based on repeated observations ($n = 16$) of appearance and disappearance of stripes (mean \pm s.e.m.). A systematic error of 7% due to inaccuracy of the setup and data acquisition is superimposed to the standard error of mean. The error in concentration was estimated by the accuracy of the magnetometer (measurement of magnetic dipole moment), sample size, and the accuracy of dry sample magnetization (also measured with the magnetometer) to around $\pm 20\%$.

The flow velocity (Figure 6b–d) was determined as the slope of the distribution of cross-correlation peak positions (as shown in Figure 6a, typical total count of 3000) using linear regression. The errors are estimated as standard errors of the regression slope. Data analysis was carried out in Origin.

Supporting Information

Supporting Information is available from the Wiley Online Library or from the author.

Acknowledgements

The authors acknowledge the financial support from the Slovenian Research Agency (research cores P1-0192, P2-0089, P1-0099 as well as projects J1-2459 and BI-AT/20-21-020) and OEAD WTZ, project number: SI 23/2020. The authors also thank the CENN Nanocenter for the use of the LakeShore 7400 Series VSM vibrating-sample magnetometer. Part of this work was performed at the Swiss spallation neutron source SINQ, Paul Scherrer Institute, Villigen, Switzerland.

Conflict of Interest

The authors declare no conflict of interest.

Data Availability Statement

The data that support the findings of this study are available from the corresponding author upon reasonable request.

Keywords

active matter, chiral symmetry breaking, ferrofluids, ferromagnetism

Received: May 25, 2023

Revised: August 4, 2023

Published online:

- [1] B. Liebchen, D. Levis, *Europhys. Lett.* **2022**, *139*, 67001.
- [2] I. H. Riedel, K. Kruse, J. Howard, *Science* **2005**, *309*, 300.
- [3] Y. Sumino, K. H. Nagai, Y. Shitaka, D. Tanaka, K. Yoshikawa, H. Chaté, K. Oiwa, *Nature* **2012**, *483*, 448.
- [4] A. P. Petroff, X.-L. Wu, A. Libchaber, *Phys. Rev. Lett.* **2015**, *114*, 158102.
- [5] G. Kokot, A. Snezhko, *Nat. Commun.* **2018**, *9*, 2344.
- [6] K. Han, G. Kokot, S. Das, R. G. Winkler, G. Gompper, A. Snezhko, *Sci. Adv.* **2020**, *6*, eaaz8535.
- [7] J.-C. Tsai, F. Ye, J. Rodriguez, J. P. Gollub, T. C. Lubensky, *Phys. Rev. Lett.* **2005**, *94*, 214301.
- [8] M. A. López-Castaño, A. Márquez Seco, A. Márquez Seco, A. Rodríguez-Rivas, F. V. Reyes, *Phys. Rev. Res.* **2022**, *4*, 033230.
- [9] C. Scholz, M. Engel, T. Pöschel, *Nat. Commun.* **2018**, *9*, 931.
- [10] C. Scholz, A. Ldov, T. Pöschel, M. Engel, H. Löwen, *Sci. Adv.* **2021**, *7*, eabf8998.
- [11] F. Afroze, D. Inoue, T. I. Farhana, T. Hiraiwa, R. Akiyama, A. M. R. Kabir, K. Sada, A. Kakugo, *Biochem. Biophys. Res. Commun.* **2021**, *563*, 73.
- [12] F. Kümmel, B. Ten Hagen, R. Wittkowski, I. Buttinoni, R. Eichhorn, G. Volpe, H. Löwen, C. Bechinger, *Phys. Rev. Lett.* **2013**, *110*, 198302.
- [13] J. Li, T. Li, T. Xu, M. Kiristi, W. Liu, Z. Wu, J. Wang, *Nano Lett.* **2015**, *15*, 4814.
- [14] P. Arora, A. K. Sood, R. Ganapathy, *Sci. Adv.* **2021**, *7*, eabd0331.
- [15] W. R. DiLuzio, L. Turner, M. Mayer, P. Garstecki, D. B. Weibel, H. C. Berg, G. M. Whitesides, *Nature* **2005**, *435*, 1271.
- [16] F. J. Maier, T. Lachner, A. Vilfan, T. O. Tasci, K. B. Neeves, D. W. M. Marr, T. M. Fischer, *Soft Matter* **2016**, *12*, 9314.
- [17] T. Barois, J.-F. Boudet, J. S. Lintuvuori, H. Kellay, *Phys. Rev. Lett.* **2020**, *125*, 238003.
- [18] V. Soni, E. S. Bililign, S. Magkiriadou, S. Sacanna, D. Bartolo, M. J. Shelley, W. T. M. Irvine, *Nat. Phys.* **2019**, *15*, 1188.
- [19] B. C. van Zuiden, J. Paulose, W. T. Irvine, D. Bartolo, V. Vitelli, *Proc. Natl. Acad. Sci. U.S.A.* **2016**, *113*, 12919.
- [20] T. Mohorič, G. Kokot, N. Osterman, A. Snezhko, A. Vilfan, D. Babič, J. Dobnikar, *Langmuir* **2016**, *32*, 5094.
- [21] M. Han, M. Fruchart, C. Scheibner, S. Vaikuntanathan, J. J. de Pablo, V. Vitelli, *Nat. Phys.* **2021**, *17*, 1260.
- [22] D. Levis, I. Pagonabarraga, B. Liebchen, *Phys. Rev. Res.* **2019**, *1*, 023026.
- [23] Z.-F. Huang, A. M. Menzel, H. Löwen, *Phys. Rev. Lett.* **2020**, *125*, 218002.
- [24] O. Petrichenko, G. Kitenbergs, M. Brics, E. Dubois, R. Perzynski, A. Cēbers, *J. Magn. Magn. Mater.* **2020**, *500*, 166404.
- [25] B. Liebchen, D. Levis, *Phys. Rev. Lett.* **2017**, *119*, 058002.
- [26] G. Kokot, S. Das, R. G. Winkler, G. Gompper, I. S. Aranson, A. Snezhko, *Proc. Natl. Acad. Sci. U.S.A.* **2017**, *114*, 12870.
- [27] C. Reichhardt, C. J. O. Reichhardt, *J. Chem. Phys.* **2019**, *150*, 064905.
- [28] H. Massana-Cid, A. Ortiz-Ambriz, A. Vilfan, P. Tierno, *Sci. Adv.* **2020**, *6*, eaaz2257.
- [29] D. Banerjee, A. Souslov, A. G. Abanov, V. Vitelli, *Nat. Commun.* **2017**, *8*, 1573.
- [30] M. Fruchart, C. Scheibner, V. Vitelli, *Annu. Rev. Condens. Matter Phys.* **2023**, *14*, 471.
- [31] C. Scheibner, A. Souslov, D. Banerjee, P. Surówka, W. T. M. Irvine, V. Vitelli, *Nat. Phys.* **2020**, *16*, 475.
- [32] T. H. Tan, A. Mietke, J. Li, Y. Chen, H. Higinbotham, P. J. Foster, S. Gokhale, J. Dunkel, N. Fakhri, *Nature* **2022**, *607*, 287.
- [33] F. Brochard, P. G. de Gennes, *J. Phys. France* **1970**, *31*, 691.
- [34] J. Rault, P. E. Cladis, J. P. Burger, *Phys. Lett. A* **1970**, *32*, 199.
- [35] B. Huke, M. Lücke, *Rep. Prog. Phys.* **2004**, *67*, 1731.
- [36] M. Shuai, A. Klitnick, Y. Shen, G. P. Smith, M. R. Tuchband, C. Zhu, R. G. Petschek, A. Mertelj, D. Lisjak, M. Čopič, J. E. MacLennan, M. A. Glaser, N. A. Clark, *Nat. Commun.* **2016**, *7*, 10394.
- [37] S. Odenbach, *Colloidal Magnetic Fluids: Basics, Development and Application of Ferrofluids*, Springer Verlag, Berlin **2009**.
- [38] W. Voit, D. K. Kim, W. Zapka, M. Muhammed, K. V. Rao, *MRS Online Proc. Libr.* **2011**, *676*, Y7.8.
- [39] A. Mertelj, D. Lisjak, M. Drofenik, M. Čopič, *Nature* **2013**, *504*, 237.
- [40] F. M. van der Kooij, K. Kassapidou, H. N. W. Lekkerkerker, *Nature* **2000**, *406*, 868.
- [41] Ž. Gregorin, N. Sebastián, N. Osterman, P. Hribar Boštjančič, D. Lisjak, A. Mertelj, *J. Mol. Liq.* **2022**, *366*, 120308.
- [42] D. Lisjak, M. Drofenik, *Cryst. Growth Des.* **2012**, *12*, 5174.
- [43] D. Makovec, B. Beleč, T. Goršak, D. Lisjak, M. Komelj, G. Dražič, S. Gyergyek, *Nanoscale* **2018**, *10*, 14480.
- [44] A. Mertelj, B. Lampret, D. Lisjak, J. Klepp, J. Kohlbrecher, M. Čopič, *Soft Matter* **2019**, *15*, 5412.
- [45] R. Eppenga, D. Frenkel, *Mol. Phys.* **2006**, *52*, 3.
- [46] P. Hribar Boštjančič, Ž. Gregorin, N. Sebastián, N. Osterman, D. Lisjak, A. Mertelj, *J. Mol. Liq.* **2022**, *348*, 118038.
- [47] C. J. Reeves, I. S. Aranson, P. M. Vlahovska, *Commun. Phys.* **2021**, *4*, 92.
- [48] S. Mühlbauer, D. Honecker, E. A. Périgo, F. Bergner, S. Disch, A. Heinemann, S. Erokhin, D. Berkov, C. Leighton, M. R. Eskildsen, A. Michels, *Rev. Mod. Phys.* **2019**, *91*, 1174.
- [49] M. Kotlarchyk, S.-H. Chen, *J. Chem. Phys.* **1983**, *79*, 2461.
- [50] K. J. Solis, J. E. Martin, *Appl. Phys. Lett.* **2010**, *97*, 034101.
- [51] K. J. Solis, J. E. Martin, *Soft. Matter.* **2012**, *8*, 11989.